phys. stat. sol. (b) **243**, No. 13, 3166–3170 (2006) / **DOI** 10.1002/pssb.200669149

Electron–phonon coupling in carbon nanotubes

M. Machón[*, 1], **S. Reich**[2], and **C. Thomsen**[1]

[1] Institut für Festkörperphysik, Technische Universität Berlin, Hardenbergstr. 36, 10623 Berlin, Germany
[2] Department of Materials Science and Engineering, Massachusetts Institute of Technology, Cambridge, Massachusetts 02139-4307, USA

Received 14 June 2006, revised 28 June 2006, accepted 1 August 2006
Published online 11 October 2006

PACS 61.46.Fg, 63.20.Kr, 63.22.+m

Knowledge of electron–phonon coupling is essential for the understanding of many properties of carbon nanotubes. We present a comparative study of the coupling of electrons to totally symmetric phonons: the radial-breathing mode and the high-energy mode. The coupling of the high-energy mode is stronger than of the radial-breathing mode by a factor of ≈6. In both cases the matrix elements depend on chirality, diameter, family, and transition energy.

1 Introduction

One of the important methods for investigating carbon nanotubes is resonance Raman spectroscopy [1]. In resonance the signal of even a single nanotube is large enough to be detected by a standard Raman setup. By scanning the laser excitation energies systematically, it has become possible to analyze the chirality of an ensemble of nanotubes in solution [2]. Carbon nanotubes with similar chiralities have slightly different transition energies and/or different radial-breathing mode frequencies, so that in a two-dimensional plot of these quantities a full separation of nanotube chiralities is possible. Photoluminescence excitation spectroscopy has been similarly successfull in this respect, with the exception that metallic nanotubes cannot be detected by this method [3].

One of the current challenges of research on phonons in nanotubes is to determine quantitatively the Raman (or luminescence) signal size theoretically. The zeroth order approximation of constant and equal matrix elements for all chirality nanotubes does not hold. In particular, we have shown for the radial-breathing mode (RBM) that there are systematic chirality dependences of the electron–phonon matrix elements for the radial-breathing mode. This finding has consequences for the determination of abundances in an ensemble of nanotubes; the relative abundancies of particular chiralities are not strictly proportional to signal size [4]. The second, and strongest mode in the Raman spectrum of carbon nanotubes is less suited for an identification of chiralities. Nevertheless, it can be used to identify a nanotube and determine whether it is metallic or semiconducting [5]. The high-energy mode (HEM) is experimentally the by far largest peak in the Raman spectrum of nanotubes, and it is therefore of interest to study theoretically the amplitude of this mode as well. In this paper we compare the electron–phonon matrix elements of the low and high-energy modes of several different chirality nanotubes by *ab initio* methods.

Many properties of solids can be explained by separate consideration of the electronic system and the core atoms, as enabled by the Born–Oppenheimer approximation. The coupling of electrons and phonons must be, however, taken into account when effects as superconductivity, transport, Raman scatter-

* Corresponding author: e-mail: maria@physik.tu-berlin.de

ing, etc, are studied. In first approximation, the electron–phonon coupling Hamiltonian can be treated as a perturbation without leaving the Born–Oppenheimer approximation.

In optical spectroscopy of carbon nanotubes, totally symmetric phonons are of special importance. A combination of the depolarization effect and Raman selection rules makes such phonons dominate the resonant spectrum. In photoluminescence, intraband relaxation can only be mediated by symmetry-preserving phonons. The optical response of carbon nanotubes is dominated by excitonic effects [6–8]. An exciton is a bound electron–hole pair, in this case created by absorption of a photon. We assume the excitonic states to follow the one-particle band-to-band transitions and approximate the exciton-phonon coupling by combining the coupling of non-correlated electrons and holes with phonons. Thus, the exciton-phonon coupling matrix element $\mathcal{M}_{\mathrm{eh},i}$ is approximated by [9, 10]

$$\mathcal{M}_{\mathrm{eh},i} \approx \mathcal{M}_i = \sqrt{\frac{\hbar}{2n_a m_C \omega_\alpha}}\ \frac{\partial E_{ii}}{\partial Q_\alpha}\ , \tag{1}$$

where $\mathcal{M}_i$ is the one-particle transition matrix element, n_a is the number of atoms in the unit cell, m_C is the carbon mass, ω_α is the frequency of the α-th normal mode. The transition deformation potential $\dfrac{\partial E_{ii}}{\partial Q_\alpha}$ is defined as

$$\frac{\partial E_{ii}}{\partial Q_\alpha} = \frac{\partial E_{ci}}{\partial Q_\alpha} - \frac{\partial E_{vi}}{\partial Q_\alpha}\ , \tag{2}$$

where $E_{c(v)i}$ is the energy of the i-th light-absorbing conduction (valence) band at density-of-states extrema. The deformation potentials $\partial E_{c(v)i}/\partial Q_\alpha$ were calculated as the slope of the linear function followed by the band energy as function of the normal mode amplitude.

Our calculations were performed with the SIESTA code [11, 12]. The parameterization of Perdew and Zunger [13] of local density approximation was used for the exchange-correlation functional. The core electrons were replaced by non-local, norm conserving pseudopotentials [14]. For the valence electrons a singly polarized double-ζ basis of localized atomic orbitals was used [15]. The basis cut-off was determined by localization corresponding to an energy shift of 50 meV. The grid cutoff in real space was 270 Ry. The reciprocal space was sampled with 16 k-points except for the (8, 4) nanotube, for which only the Γ point was used. Each nanotube was relaxed until the forces were less than 0.04 eV/Å, the normal modes were calculated with the method of finite differences.

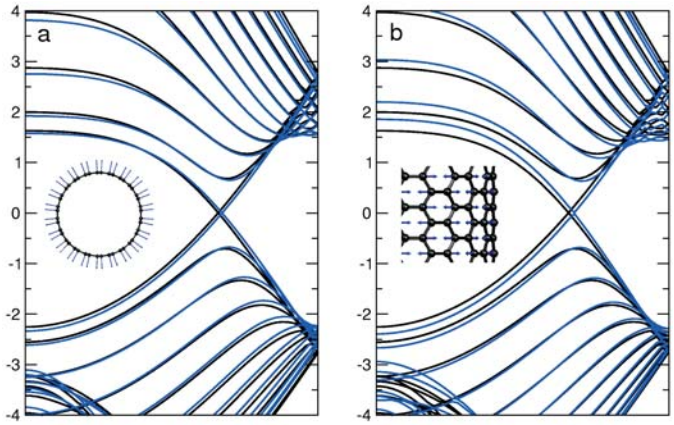

Fig. 1 (online colour at: www.pss-b.com) Band structure of the (11, 11) nanotube in the relaxed geometry (black lines), and deformed after the displacement pattern shown, which corresponds to: (a) RBM, displacement magnitude 0.142 Å; (b) HEM, displacement magnitude 0.02 Å.

Table 1 RBM and HEM (graphite-E_{2g}-derived-modes) frequencies (in cm^{-1}) and electron–phonon coupling matrix elements (in meV). The index i in $\mathcal{M}_i$ indicates the four first optical transitions for each nanotube. The "*" indicates a negligible matrix element; a "–" indicates a matrix element which could not be extracted from the calculations.

				$\mathcal{M}_1$		$\mathcal{M}_2$		$\mathcal{M}_3$		$\mathcal{M}_4$	
	ω^{rbm}	ω^{ax}	ω^{circ}	rbm	hem	rbm	hem	rbm	hem	rbm	hem
(6,6)	**278**	1563	**1626**	−15	−85	–	–	–	–	–	–
(8,8)	**230**	1564	**1619**	−10	−53	−15	−84	−15	−93	–	–
(11,11)	**151**	1571	**1602**	−5	*	−10	−66	−12	−79	–	–
(8,4)	**274**	**1670**	**1505**	−13	−31 71	4	−22 −66	−16	−25 83	–	– –
(6,0)	**446**	**1587**	1490	50	−152	−62	171	–	–	–	–
(10,0)	**287**	**1627**	1590	−28	130	17	−110	−30	148	−31	151
(14,0)	**203**	**1636**	1610	16		−20		−21		–	–
(15,0)	**188**	**1567**	1579	−22	117	13	−88	−22	128	−22	134
(16,0)	**179**	**1635**	1614	−17		13		−18		–	–
(17,0)	**170**	**1635**	1613	14	−89	−16	100	−17	111	9	−78
(19,0)	**149**	**1635**	1614	−15	94	12	−83	−16	104	−16	112

We first take a look at the (11, 11) armchair nanotube. Its calculated equilibrium band structure is displayed in Fig. 1 (black lines). We then add a phonon displacement vector to the equilibrium structure and re-calculate the bandstructure. The blue (gray) lines in Fig. 1(a) correspond to the nanotube with the pattern of the radial breathing mode and the totally symmetric high-energy mode (b) superimposed. The vertical displacement of the bands differs throughout the Brillouin zone, but is a linear function of the atomic displacement for each k. From the slope of this linear function we obtain the deformation potentials of Eq. (2). From Fig. 1 we can conclude the following features which hold similarly for the other nanotubes studied: Aside from the k-vector dependence of the deformation potentials their sign also depends on k, and for a given k-point they are much larger for the high-energy mode than for the radial-breathing mode.

In Table 1 we present all of our results. We list the first four transition matrix elements for the high-energy and the radial-breathing mode and find confirmed that for every nanotube the coupling with the high-energy mode is stronger than with the low-energy mode. There is an exception: the $\mathcal{M}_1$ matrix element of the first transition of the (11, 11) nanotube. For this transition, the HEM matrix element turned out negligible in our calculation as compared to the RBM. To find a physical reason for this exception, let us take a look back at Fig. 1(b). We see that the displaced bands intersect or cross the equilibrium bands at particular wave vectors close to the Fermi point k_F at $\approx 2/3$ of the Brillouin zone. In such a point the deformation potential is zero, hence for optical transitions occurring at or near those points the electron–phonon matrix element is small or negligible. Such an intersection or node is common to all armchair nanotubes. From the zone-folding approximation to the band structure we know that the extrema of the bands of armchair nanotubes move closer to k_F for decreasing transition energies. At small enough transition energies the band extrema are quite close to the node of displaced and undisplaced bands and the electron–phonon coupling strength vanishes [16].

For zigzag nanotubes in Table 1 we see a sign and magnitude alternation of the matrix elements of both low and high-energy modes. We were able to explain this behavior for the radial-breathing mode with a zone-folding model of graphene, a single layer of graphite [10]. The explanation is also valid for the high-energy mode, since it relies on a general property of zigzag carbon nanotubes. For states at k points which can be mapped back on the interior of the Brillouin zone of graphene, the graphene π band corresponds to the valence band of the nanotube, and the π^* to the conduction band. This is inverted for

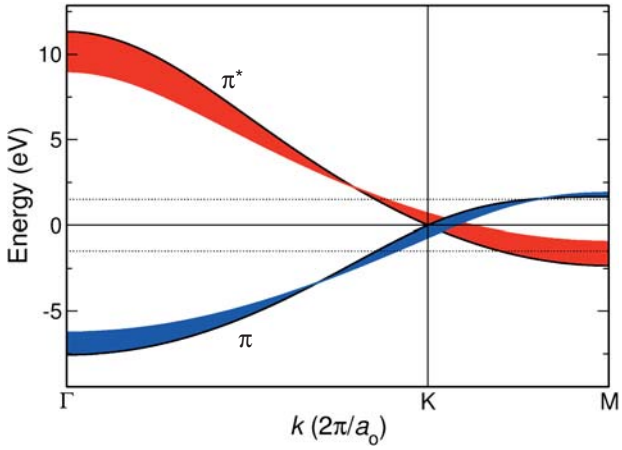

Fig. 2 (online colour at: www.pss-b.com) Electronic bands of graphene along Γ–K–M in equilibrium (solid black line) and under a deformation of 0.1 Å corresponding to the RBM of a (19, 0) tube (colored area, difference enhanced ×10).

states from outside the Brillouin zone of graphene. In Fig. 2 the calculated π and π* bands of graphene along the Γ–K–M line are shown. The black lines correspond to the relaxed geometry. The colored areas indicate the change of the electronic bands when translating the atoms of graphene simulating the radial-breathing mode of a (19, 0) nanotube. We included the non-radial component of the mode, which corresponds to an in-plane component in the graphene model. The π and π* bands of graphene shift continuously under the effect of the atomic displacement, without sign change within the boundaries of the K-point, relevant for optical transitions in the visible range (between the dotted lines). There is, thus, a discontinuity in the sign of the electron–phonon coupling deformation potentials at the K-point of graphite, which gives rise to the sign alternation. The same is found for the high-energy mode, which explains the sign alternation for both modes.

In Fig. 3 we show the sign alternation explicitly. Here we entered the deformation potentials at the k-points along Γ–K–M, where their transitions occur when mapped onto the Brillouin zone of graphene. The colored points correspond to different-diameter nanotubes of zig-zag and armchair type as indicated. We plotted the deformation potential as defined in Eq. (2) including their sign. Same colored points

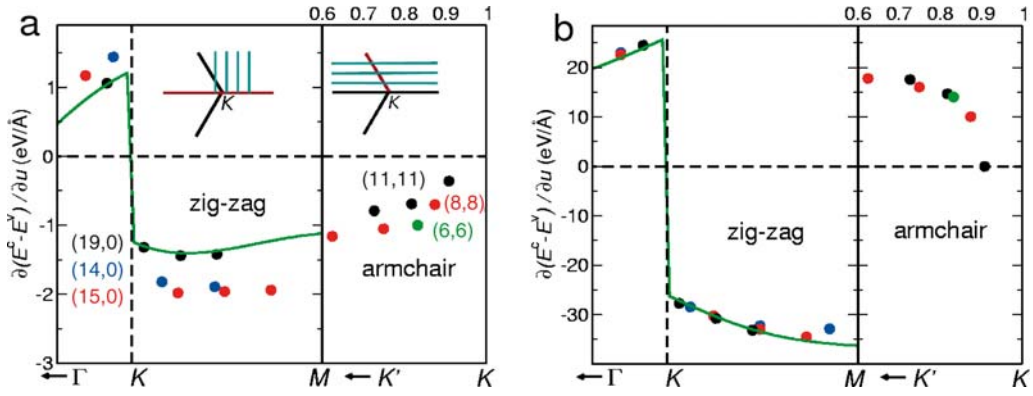

Fig. 3 (online colour at: www.pss-b.com) Deformation potentials calculated for several armchair and zig-zag nanotubes (dots) compared to a zone-folding calculation of graphite (solid line). (a) for the radial-breathing mode and (b) for the high-energy mode. The colors are defined by the labels in (a). After Ref. [10].

belong to different transitions (and hence bands) of a nanotube. The lowest optical transition, e.g., of the (19, 0) nanotube corresponds to the point closest to the K-point and to the right of it. It has a negative sign. The deformation potential $\mathcal{M}_2$ of the second transition is marked by the black point to the left of the K-point; its sign is positive, and so on. The other tubes show a corresponding behavior. For armchair nanotubes we follow the systematic decrease of the matrix elements as we approach the K-point (see also the inset). Strictly at the K-point the matrix elements vanish because of the node, see discussion above. Similar results are found for the high-energy mode in Fig. 3(b). Note, however, that the magnitude of the deformation potential is larger by about one order of magnitude than those in (a). In the RBM we observe a direct diameter dependence of the deformation potentials not found for the HEM.

Recent tight-binding calculations of the Raman intensities of the $A_{1(g)}$ phonons in nanotubes agree qualitatively with our results [17]. There is a nice agreement between both levels of theory with respect to the relative intensity of the HEM and RBM. The dependence of the Raman intensity on chiral angle, diameter, and family follows similar trends as found in our calculations of $\mathcal{M}_{e-ph}$. Further comparison is, however, not possible since the electron–phonon matrix elements are not given explicitely in Ref. [17].

In conclusion, we calculated and compared the electron–phonon coupling matrix elements for the radial-breathing mode and the high-energy mode of 11 different carbon nanotubes. We found a systematic dependence of the magnitude and sign for different optical transitions. We could explain the dependences on the basis of where in the Brillouin zone the transitions occurred. Generally the high-energy mode has an about one order of magnitude larger matrix element than the radial-breathing mode. For the detection of nanotubes the HEM is thus more suitable than the RBM, while the latter remains indispensible for the chirality identification. The analysis of relative abundances must be treated with care as the assumption of equal signal size for all types of tubes is not warranted. The difference in electron–phonon matrix elements reported here has to be further convolved with the optical matrix elements before arriving at definite conclusions concerning the abundances from a Raman (or luminescence) experiment.

References

[1] S. Reich, C. Thomsen, and J. Maultzsch, Carbon Nanotubes, Basic Concepts and Physical Properties (Wiley-VCH, Berlin, 2004).
[2] H. Telg, J. Maultzsch, S. Reich, F. Hennrich, and C. Thomsen, Phys. Rev. Lett. **93**, 177401 (2004).
[3] S. M. Bachilo, M. S. Strano, C. Kittrel, R. H. Hauge, R. E. Smalley, and R. B. Weisman, Science **298**, 2361 (2002).
[4] H. Telg, J. Maultzsch, S. Reich, F. Hennrich, and C. Thomsen, phys. stat. sol. (b) **243**(13), (2006) (this issue).
[5] J. Maultzsch, S. Reich, C. Thomsen, H. Requardt, and P. Ordejón, Phys. Rev. Lett. **92**, 075501 (2004).
[6] C. D. Spataru, S. Ismail-Beigi, L. X. Benedict, and S. G. Louie, Phys. Rev. Lett. **92**, 077402 (2004).
[7] F. Wang, G. Dukovic, L. E. Brus, and T. F. Heinz, Science **308**, 838 (2005).
[8] J. Maultzsch, R. Pomraenke, S. Reich, E. Chang, D. Prezzi, et al., Phys. Rev. B **72**, 241402 (2005).
[9] F. Khan and P. Allen, Phys. Rev. B **29**, 3341 (1984).
[10] M. Machón, S. Reich, H. Telg, J. Maultzsch, P. Ordejón, and C. Thomsen, Phys. Rev. B **71**, 035416 (2005).
[11] P. Ordejón, E. Artacho, and J. M. Soler, Phys. Rev. B **53**, 10441(R) (1996).
[12] J. M. Soler, E. Artacho, J. D. Gale, A. García, J. Junquera, P. Ordejón, and D. Sánchez-Portal, J. Phys.: Condens. Matter **14**, 2745 (2002).
[13] J. P. Perdew and A. Zunger, Phys. Rev. B **23**, 5048 (1981).
[14] N. Troullier and J. Martins, Phys. Rev. B **43**, 1993 (1991).
[15] J. Junquera, O. Paz, D. Sánchez-Portal, and E. Artacho, Phys. Rev. B **64**, 235111 (2001).
[16] M. Machón, S. Reich, and C. Thomsen, Strong electron–phonon coupling of the high-energy modes of carbon nanotubes, submitted to Phys. Rev. B (2006).
[17] V. N. Popov and P. Lambin, Phys. Rev. B **73**, 165425 (2006).

